

Energy-Efficient Channel Decoding for Wireless Federated Learning: Convergence Analysis and Adaptive Design

Linping Qu, *Graduate Student Member, IEEE*, Yuyi Mao, *Member, IEEE*,
Shenghui Song, *Senior Member, IEEE*, and Chi-Ying Tsui, *Senior Member, IEEE*

Abstract—One of the most critical challenges for deploying distributed learning, such as federated learning (FL), in wireless networks is the limited battery capacity of mobile devices. While it is a common belief that the major energy consumption of mobile devices comes from the uplink data transmission, this paper presents a novel finding, namely the channel decoding operation also contributes significantly to the overall energy consumption of mobile devices in FL. Motivated by this new observation, we propose an energy-efficient adaptive channel decoding scheme that leverages the intrinsic robustness of FL to model errors. In particular, the robustness is exploited to reduce the energy consumption of channel decoders at mobile devices by adaptively adjusting the number of decoding iterations. We theoretically prove that FL with communication errors can converge at the same rate as error-free communication as long as the bit error rate (BER) is properly constrained. An adaptive channel decoding scheme is then proposed to improve the energy efficiency of FL systems. Experimental results demonstrate that the proposed method maintains the same learning accuracy while reducing the channel decoding energy consumption by 20% when compared to existing approaches.

Index Terms—Federated learning (FL), energy efficiency, channel decoding, low-density parity checking (LDPC), bit error rate (BER).

I. INTRODUCTION

A. Motivation

Deep learning has achieved remarkable success in numerous realms, such as computer vision and natural language processing [1]. However, the conventional centralized learning paradigm encounters the data isolation issue due to the rising concern about privacy [2]. As a result, uploading the distributed data, which may contain privacy-sensitive information, for centralized learning becomes prohibited. To address this issue, federated learning (FL) was proposed [3] to enable the training of deep learning models without sharing the data of users (e.g., IoT devices). However, to fully unlock the

potential of FL, we need to tackle several critical challenges, such as data and device heterogeneity [4]–[6], as well as the communication bottleneck [7]. Another issue for wireless FL is the energy consumption of mobile devices due to heavy computation and communication workloads for training and transferring the deep neural network (DNN) parameters [8].

Many innovative approaches have been proposed to reduce the energy consumption of mobile devices in FL from different perspectives. For instance, reinforcement learning was utilized in [9] to identify a near-optimal clustering of participating devices to reduce the overall energy consumption of mobile devices. In [10], the trade-off between learning accuracy and users' total energy consumption was optimized through computational and communication resource allocation. Besides system-level resource management, some works focused on the power consumption of specific hardware components such as transmitters, receivers, and artificial intelligence (AI) chips. Techniques such as model sparsification [11] and quantization [12]–[17] have been proposed to minimize the communication overhead, thus reducing the energy consumption of the transmitters. The authors of [18] and [19] minimized the transmission energy while maintaining the learning performance. From computation perspective, model sparsification and quantization techniques are also beneficial for minimizing the processing energy consumption [20]–[22]. Additionally, some works, such as [10], [23], and [24], considered the joint optimization of the uplink transmission and local training energy consumption. However, very few works have paid attention to the energy consumption of channel decoder. As will be shown in Section II-B, channel decoders consume a substantial portion of energy because of the iterative process to decode massive DNN parameters.

To address the research gap, in this work, we first quantitatively analyze the energy consumption of different components in mobile clients and show that the channel decoder contributes significantly to the overall energy consumption. Building on this observation, an energy-efficient channel decoding strategy is designed for wireless FL systems, by leveraging the fact that FL is robust to model errors due to its statistical learning nature [25]. Furthermore, we conduct a theoretical analysis on the relation between the bit error rate (BER) and the convergence rate of FL, and determine the maximum tolerable BER that can maintain the same convergence rate as the case with error-free communication. Finally, we propose a practical approach to adjust the decoding iterations in each communication round

This work was partially supported by AI Chip Center for Emerging Smart System (ACCESS) sponsored by InnoHK funding, Hong Kong, SAR, and partially supported by a grant from the NSFC/RGC Joint Research Scheme sponsored by the Research Grants Council of the Hong Kong Special Administrative Region, China and National Natural Science Foundation of China (Project No. N_HKUST656/22).

Linping Qu, Shenghui Song, and Chi-Ying Tsui are with the Department of Electronic and Computer Engineering, Hong Kong University of Science and Technology, Hong Kong (e-mail: lqu@connect.ust.hk; eeshsong@ust.hk; eetsui@ust.hk). Yuyi Mao is with the Department of Electrical and Electronic Engineering, Hong Kong Polytechnic University, Hong Kong (e-mail: yuyi-eie.mao@polyu.edu.hk).

to achieve the maximum tolerable BER, while reducing the energy consumption.

B. Contributions

This paper investigates the impact of channel decoding on the energy consumption of wireless FL. The major contributions are summarized as follows:

- We theoretically analyze the relation between BER and the convergence rate of FL. The maximum tolerable BER to achieve the same convergence rate as error-free FL is determined.
- Based on the analysis, an adaptive low-density parity checking (LDPC) decoding mechanism is proposed, which controls the maximum number of decoding iterations to reduce the energy consumption of wireless FL while satisfying the BER requirement for a target convergence rate.
- Experimental results show that the proposed adaptive scheme effectively reduces the energy consumption by 20% when compared with the traditional scheme, while guaranteeing the same learning performance.

C. Organization

The remainder of this paper is organized as follows. Section II introduces the system model and presents a comprehensive energy consumption analysis for mobile devices. Section III develops an energy-efficient LDPC decoding strategy for FL systems by exploiting the relationship between the convergence rate of FL and the achieved BER of LDPC decoding. Experimental results are presented in Section IV. Finally, concluding remarks are drawn in Section V.

II. SYSTEM MODEL AND PRELIMINARIES

In this section, we first introduce the wireless FL system. An overview regarding the energy consumption of different components at a mobile unit is then presented, which highlights the significant contribution of channel decoding to the total energy consumption of wireless FL. For ease of reference, we list the key notations of the system model in Table I.

A. Wireless FL

Fig. 1 depicts a wireless FL system, where model training of different clients is coordinated by the server. The FL problem can be formulated as follows [26]–[28]:

$$\min_{\mathbf{w} \in \mathbb{R}^d} f(\mathbf{w}) \triangleq \sum_{k=1}^n p_k f_k(\mathbf{w}), \quad (1)$$

where \mathbf{w} denotes the model parameters, n represents the number of clients, p_k is the ratio between the amount of training data samples of the k -th client and that of all the clients, and $f_k(\mathbf{w})$ is the local loss function of the k -th client.

To train a shared global model, the server communicates with the mobile clients for multiple rounds through noisy wireless channels. In each communication round, the global model at the server is broadcast to a set of selected clients. Each of the selected clients then performs local training

TABLE I: Key Notations

Notation	Definition
\mathbf{w}	DNN model.
$\Delta \mathbf{w}$	The local model update.
f	The loss function of training.
f^*	The minimum value of the training loss.
∇f	The gradient.
r	The index of the communication round.
R	The total communication rounds.
e	The index of the local training step.
E	The local training steps.
σ_L^2	The variance of local gradients estimator.
σ_G^2	The dissimilarity between local and global gradients.
k	The index of the mobile device.
n	The number of total mobile devices.
s	The number of selected clients in every round
S_r	The set of selected clients in the r -th round.
d	The dimensions of the DNN model.
p_k	The data size ratio of the k -th client.
T	The total training iterations of one client.
L	The L-smooth parameter.
b_r	The bit error rate in r -th communication round.
η	The learning rate.
M	The biggest absolute weight value.
Q	The LDPC maximum decoding iteration.

based on the received global model and transmits the model updates to the server for aggregation. Specifically, in the r -th communication round, the global model is quantized by a stochastic quantizer, encoded by a channel code, and broadcast to clients. The model parameters received by the k -th client is given as follows:

$$\mathbf{w}_{r,0}^k = \mathbf{w}'_r, \quad (2)$$

where \mathbf{w}'_r denotes the noisy version of \mathbf{w}_r . The impact of BER can be quantified by considering different error bit positions in the model parameters and the detailed analysis is given in Appendix B. A selected client updates the received global model by conducting E steps of local mini-batch Stochastic Gradient Descent (SGD) with a learning rate η as follows:

$$\mathbf{w}_{r,e+1}^k = \mathbf{w}_{r,e}^k - \eta \nabla f_k(\mathbf{w}_{r,e}^k, \xi), e = 0, \dots, E-1, k \in S_r, \quad (3)$$

where $\nabla f_k(\mathbf{w}_{r,e}^k, \xi)$ denotes the gradient computed from the local mini-batch datasets ξ in the k -th client, and S_r denotes the set of selected clients in the r -th communication round.

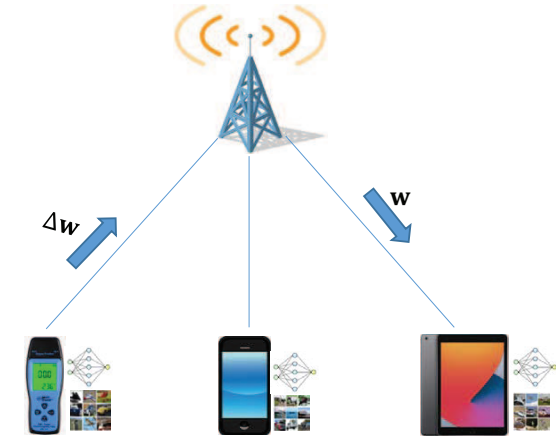
By completing E steps of local training, the local model update of the k -th client can be expressed as follows:

$$\Delta \mathbf{w}_r^k = \mathbf{w}_{r,E}^k - \mathbf{w}_{r,0}^k, \quad (4)$$

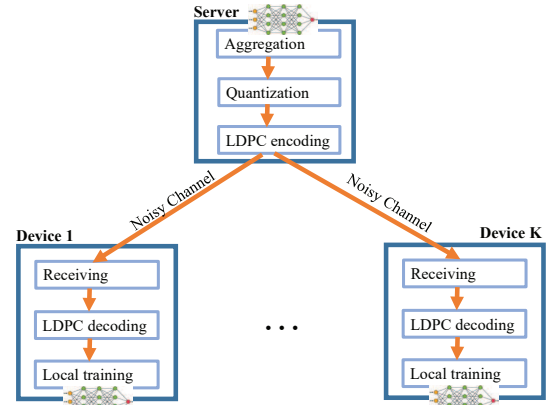
which is quantized, encoded, and uploaded to the server. For simplicity, we assume an orthogonal uplink channel is available for each selected client. After receiving these noisy local updates, denoted as $(\Delta \mathbf{w}_r^k)'$, the server performs aggregation to update the global model as follows:

$$\mathbf{w}_{r+1} = \mathbf{w}_r + \frac{1}{|S_r|} \sum_{k \in S_r} p_k (\Delta \mathbf{w}_r^k)'. \quad (5)$$

In this work, we focus on the downlink communication rather than the uplink for two reasons. First, our objective is to design channel decoding schemes to save the energy



(a) Wireless FL system. Multiple mobile clients are coordinated by one remote server through the noisy wireless channels. The communicated parameters are model updates in the uplink and model weights in the downlink.



(b) System operations. Server: aggregation, quantization, LDPC encoding, client selection and broadcasting. Mobile devices: receiving model weights, LDPC decoding, local training and uplink transmission.

Fig. 1: Wireless FL in digital communication, system outlook and underlying operations.

consumption of mobile devices. For the uplink, the channel decoding happens on the server side which falls out of the scope of this study. Second, the server has a continuous power supply and is able to conduct a sufficient number of decoding iterations to achieve satisfactory BER performance.

B. Energy Consumption Evaluation

There are two main energy-consuming operations for clients participating in wireless FL, namely model training and model communication. For the latter, it is believed that the energy is mostly consumed by the data transmission. In this section, we evaluate the energy consumption of different components, taking the training of AlexNet for image classification tasks as an example [29]. The analysis is based on actual measurements obtained from fabricated chips published in recent years [30]–[32]. For fair comparisons, all data are collected for chips fabricated in the 65 nm complementary metal-oxide semiconductor (CMOS) process.

In [30], a fabricated AI hardware accelerator was reported to achieve the energy efficiency of 13.7 mJ/epoch for 8-bit quantized AlexNet. With five epochs of local training, the processing energy consumption in each communication round is 68.5 mJ. In [31], a fifth-generation (5G) New Radio wireless transmitter and receiver were reported to achieve the energy efficiencies of 47.9 pJ/b and 33.3 pJ/b for transferring uncoded data, respectively, under a communication distance of around 200 meters. Therefore, the energy required to transmit and receive the 8-bit AlexNet with 60 million parameters in a single communication round is about 39 mJ. Assuming a code rate of 1/2, the communication energy consumption for coded transmission of the AlexNet model parameters in each round is 78 mJ. Besides, the LDPC decoder in [32] achieves the energy efficiency of 20.1 pJ/b/iteration, which was measured with 10 decoding iterations on average. Accordingly, the energy consumption of the LDPC decoder for decoding the AlexNet model parameters is 96.5 mJ. The detailed comparison is presented in Table II, which indicates that the energy consumption

TABLE II: Energy Consumption of Main Components at a Mobile Unit in Wireless FL for Training an AlexNet

Component	Energy efficiency	Energy consumption
AI Chip	13.7 mJ/epoch [30]	68.5 mJ
RF Transceiver	81.2 pJ/b [31]	78 mJ
LDPC Decoder	20.1 pJ/b/iter [32]	96.5 mJ

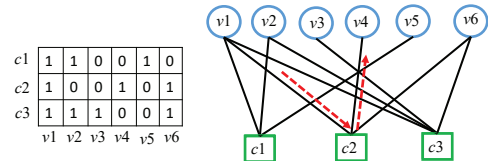


Fig. 2: Typical LDPC decoder architecture: the variable nodes and check nodes are connected, and the messages are transmitted between them iteratively.

of LDPC decoding accounts for a large portion of the overall energy consumption in wireless FL.

C. LDPC Decoding

In this work, we use LDPC codes as an example to illustrate how adaptive channel decoding can help reduce the energy consumption of wireless FL. To that end, we first introduce a typical LDPC decoder architecture in Fig. 2, which contains the variable nodes representing the encoded bits to be corrected and check nodes representing the parity check equation. The check nodes exchange information with variable nodes and perform computations iteratively until achieving the maximum decoding iteration [33]. Such iterative processing leads to high energy consumption of LDPC decoding. To save decoding energy, early termination techniques are usually adopted. Specifically, if the parity-check matrix \mathbf{H} and the codeword \mathbf{x} satisfy $\mathbf{H}\mathbf{x}^T = 0$, the decoding process will stop even if the maximum decoding iteration has not been reached [34]. The early termination scheme can save decoding

iterations while preserving BER performance. The energy consumption of LDPC decoding depends on the target BER. As a result, to minimize the energy consumption, it is essential to determine the maximum tolerable BER by FL systems, considering its unique statistical learning nature.

III. ENERGY-EFFICIENT LDPC DECODING DESIGN

In this section, we propose an energy-efficient LDPC decoding scheme to minimize the decoding energy consumption while guaranteeing the same convergence rate for wireless FL as the case with error-free communication. For that purpose, we explore the relationship between BER and convergence rate, and that between the maximum number of decoding iterations and BER. By connecting these two relationships, we demonstrate how to regulate the LDPC decoding scheme.

A. Effect of BER on the Convergence Rate of Wireless FL

With error-free communication, the convergence rate of FL with non-convex loss functions is proved as $\mathcal{O}(1/\sqrt{T})$ [35], where T is the total number of training epochs. In this subsection, we investigate how BER affects the convergence rate of FL and determine the maximum admissible BER for maintaining the convergence rate of $\mathcal{O}(1/\sqrt{T})$.

Unlike FL with analog communication [36]–[42], quantifying the impact of BER on FL with digital communication is not straightforward. In particular, we need to consider different cases of bit errors and analyze the impact of different bit errors, e.g., most significant bits and least significant bits.

To conduct the theoretical analysis, we take the following assumptions that are widely adopted in the literature.

Assumption 1. (*L-Smoothness* [12], [35]) *The local loss function $f_k(\cdot)$ at the k -th client is L -smooth, i.e., $\forall \mathbf{w}, \hat{\mathbf{w}}$, we have $\|\nabla f_k(\mathbf{w}) - \nabla f_k(\hat{\mathbf{w}})\| \leq L\|\mathbf{w} - \hat{\mathbf{w}}\|$.*

Assumption 2. (*Unbiased and Bounded-variance Local Gradient Estimator* [43]) *Let ξ_r^k be the batch of randomly sampled data at the k -th client in the r -th communication round. The gradient estimator $\nabla f_k(\mathbf{w}; \xi_r^k)$ is unbiased, i.e., $\mathbb{E}[\nabla f_k(\mathbf{w}; \xi_r^k)] = \nabla f_k(\mathbf{w})$, and has a bounded variance, i.e., $\mathbb{E}[\|\nabla f_k(\mathbf{w}; \xi_r^k) - \nabla f_k(\mathbf{w})\|^2] \leq \sigma_L^2$.*

Assumption 3. (*Bounded Local and Global Gradient Dissimilarity* [43]) *The global dissimilarity between the local and global gradient is bounded, i.e., $\|\nabla f_k(\mathbf{w}) - \nabla f(\mathbf{w})\|^2 \leq \sigma_G^2$.*

Assumption 4. (*Unbiased Quantization* [12], [28], [35]) *The random quantizer $Q(\cdot)$ is unbiased, i.e., $\mathbb{E}[Q(\mathbf{w})|\mathbf{w}] = \mathbf{w}$.*

With **Assumptions 1-4**, the convergence bound of wireless FL with a given BER is given by the following theorem.

Theorem 1. *When the learning rate is set as $\eta = \frac{1}{L\sqrt{RE}} = \frac{1}{L\sqrt{T}}$, the average expected squared norm of global stochastic gradient is bounded as follows:*

$$\begin{aligned} & \frac{1}{T} \sum_{r=1}^R \sum_{e=1}^E \mathbb{E} \|\nabla f(\bar{\mathbf{w}}_{r,e})\|^2 \\ & \leq \frac{C_0}{\sqrt{T}} + \frac{C_1 \sum_{r=1}^R b_r}{\sqrt{T}} + \frac{C_2}{\sqrt{T}} + \frac{C_3}{\sqrt{T}}, \end{aligned} \quad (6)$$

where $\bar{\mathbf{w}}_{r,e} \triangleq \frac{1}{n} \sum_{k=1}^n \mathbf{w}_{r,e}^k$, $C_0 \triangleq 2L(f(\mathbf{w}_0) - f^*)$, $C_1 \triangleq \frac{8L^2 dM^2}{3}$, $C_2 = \sigma_L^2 \left(\frac{1}{n} + \frac{4(n-s)}{s(n-1)}\right)$, $C_3 \triangleq \frac{\sigma_G^2}{L}$, f^* is the minimum global training loss, b_r is the BER in the r -th communication round, and \mathbf{w}_0 is the initial global model.

Proof. The key idea is to first quantify the BER's impact on the model error and then introduce the model error to the convergence analysis of vanilla learning process. The detailed proof is available in the Appendix. \square

Remark 1. *It is worthy noting that the first term on the right-hand side (RHS) of (6) captures the difference between the initial and minimum global training loss. The second term indicates how bit errors in each communication round affect learning convergence. The third term comes from the random mini-batch sampling and partial client participation, and the fourth term shows the impact of imbalanced data distribution.*

According to **Theorem 1**, in order to guarantee the convergence rate of $\mathcal{O}(1/\sqrt{T})$, it is crucial to control the BER in each communication round. Although the explicit relation between b_r and r is difficult to obtain, we know from the above discussion that, b_r should be a decreasing function with r as otherwise the second term on the RHS of (6) cannot be diminished with T increases. For ease of implementation, we propose a simple BER regulation with $b_r \propto \frac{1}{r^2}$, which is shown in the following corollary as a sufficient condition for a practical wireless FL system to achieve the same convergence rate as that with error-free communication.

Corollary 1. *If the BER in each communication round is regulated as follows:*

$$b_r \propto \frac{1}{r^2}, r = 1, 2, \dots, R, \quad (7)$$

the RHS of (6) diminishes to zero at the rate of $\mathcal{O}(1/\sqrt{T})$, i.e., wireless FL converges to a local optimal solution of the global training loss function at a rate of $\mathcal{O}(1/\sqrt{T})$.

Proof. To prove the RHS of (6) diminishes to zero at the rate of $\mathcal{O}(1/\sqrt{T})$, it is sufficient to verify

$$\lim_{T \rightarrow \infty} \frac{\sum_{r=1}^R b_r}{\sqrt{T}} = 0 \quad (8)$$

when $b_r \propto 1/r^2 \triangleq \delta/r^2$. Since

$$\begin{aligned} 0 & \leq \frac{\sum_{r=1}^R b_r}{\sqrt{T}} = \delta \frac{\sum_{r=1}^R 1/r^2}{\sqrt{T}} \\ & = \frac{\delta}{\sqrt{T}} \left(1 + \sum_{r=2}^R \frac{1}{r^2} \right) \\ & < \frac{\delta}{\sqrt{T}} \left(1 + \sum_{r=2}^R \frac{1}{r(r-1)} \right) = \frac{\delta}{\sqrt{T}} \left(2 - \frac{1}{R} \right) \\ & = \frac{\delta}{\sqrt{T}} \left(2 - \frac{E}{T} \right), \end{aligned} \quad (9)$$

we conclude (8) by letting $T \rightarrow \infty$ for both sides of (9) and applying the Sandwich Theorem. \square

Corollary 1 indicates that gradually decreasing the BER at a rate of $\mathcal{O}(1/r^2)$ can guarantee the convergence rate of wireless

Algorithm 1: Regulating LDPC decoder in FL

```

1 Input: The initial global model  $\mathbf{w}_0$ 
2 Output: The converged global model  $\mathbf{w}_R$ 
3 for Communication round  $r = 1, 2, \dots, R$  do
4   for Client index  $k$  in  $\{1, 2, \dots, K\}$  do
5      $b_r \propto (1/r^2)$  with  $b_1, b_R$ 
6      $Q = f^{-1}(b_r)$ 
7     for  $\text{decoding.iter} \leq Q$  do
8       one iteration of LDPC decoding
9       if Early termination is satisfied then
10        | break
11       end
12        $\text{decoding.iter} + = 1$ 
13     end
14     output:  $\mathbf{w}'_r$ 
15     for local training step  $e = 1, \dots, E$  do
16       |  $\mathbf{w}_{r,0}^k = \mathbf{w}'_r$ 
17       |  $\mathbf{w}_{r,e+1}^k = \mathbf{w}_{r,e}^k - \eta_r \nabla f(\mathbf{w}_{r,e}^k)$ 
18     end
19      $\Delta \mathbf{w}_r^k = \mathbf{w}_{r,E}^k - \mathbf{w}_{r,0}^k$ 
20   end
21    $\mathbf{w}_{r+1} = \mathbf{w}_r + \sum_{k=1}^K p_k \Delta \mathbf{w}_r^k$ 
22 end

```

FL at a rate of $\mathcal{O}(1/\sqrt{T})$. The proposed BER scaling rule achieves an improving communication quality with communication rounds. This is consistent with the solution developed in [40], which improves the communication quality by increasing the signal-to-noise ratio (SNR) with communication round.

B. BER vs. Number of Iterations

The analysis in Section III-A indicates that the convergence rate of wireless FL with error-free communication can be achieved if the BER is properly controlled. In this subsection, we analyze the relationship between BER and the maximum number of LDPC decoding iterations, based on which, we develop an adaptive decoding scheme to maintain the same convergence rate. It has been shown in [44] that for message-passing-based channel decoders to achieve a fraction of $1-\epsilon$ of the channel capacity over a binary erasure channel, the relationship between the decoding complexity (denoted as χ_D) and BER (denoted as b) can be modeled as follows:

$$\chi_D = \mathcal{O}\left(\log \frac{1}{b}\right) + \mathcal{O}\left(\frac{1}{\epsilon} \log \frac{1}{\epsilon}\right). \quad (10)$$

According to [45], the relationship between the decoding complexity and the maximum number of decoding iterations (Q) can be modeled as follows:

$$\chi_D = Q \cdot \chi_0, \quad (11)$$

where χ_0 denotes the decoding complexity per iteration. By combining (10) and (11), it leads to the following relationship between the maximum number of decoding iterations and BER:

$$Q = \frac{1}{\chi_0} \mathcal{O}\left(\log \frac{1}{b}\right) + \frac{1}{\chi_0} \mathcal{O}\left(\frac{1}{\epsilon} \log \frac{1}{\epsilon}\right). \quad (12)$$

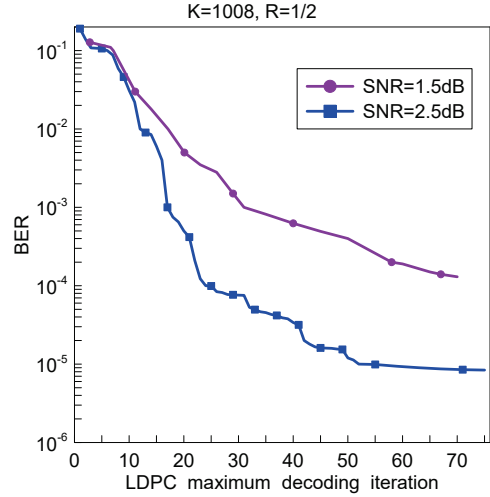


Fig. 3: The relation between BER and LDPC maximum decoding iterations under different SNRs.

In the next subsection, we develop an adaptive scheme to control the maximum number of decoding iterations for clients in a wireless FL system based on **Corollary 1** and (12).

C. Decoding Iteration Control

In this subsection, we show how to adaptively control the maximum number of LDPC decoding iterations over communication rounds to achieve the desired BER.

In principle, by combining (7) and (12), we obtain the following relationship between the maximum number of LDPC decoding iterations and communication rounds:

$$Q_r = \frac{1}{\chi_0} \mathcal{O}(2 \log r) + \frac{1}{\chi_0} \mathcal{O}\left(\frac{1}{\epsilon} \log \frac{1}{\epsilon}\right), \quad (13)$$

which provides a guideline to select the maximum number of LDPC decoding iterations in the r -th communication round. Specifically, Q_r can be set as $\alpha \log r + \beta$, where α and β are constants. However, (13) cannot be directly utilized because α and β are code-specific and depend on the receive SNR as well as channel decoding algorithms. Thus, we propose a practical approach by a lookup table, which captures the relationship between BER and the maximum number of decoding iterations at different levels of receive SNR. Entries in the lookup table can be obtained through empirical measurements specific to the LDPC code used in the wireless FL system. Fig. 3 shows the sample simulation results for a rate 1/2 LDPC code with a block length of 1008 bits and binary phase shift keying (BPSK) modulation over an additional white Gaussian noise (AWGN) channel with SNR = 1.5 and 2.5 dB. Data in this figure can be stored in a three-dimensional lookup table [46]. From the lookup table, we can get the corresponding maximum number of decoding iteration for a target BER for clients with different receive SNR.

The wireless FL procedures with adaptive LDPC decoding are summarized in Algorithm 1. The algorithm starts with an initial target BER, denoted as b_0 , which is set to a relatively high value, i.e., 10^{-1} in our experiments. The target BER at

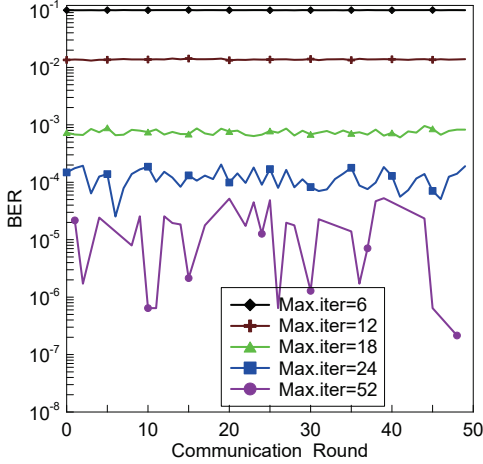


Fig. 4: Fixed decoding schemes: On the mobile side, setting the LDPC maximum decoding iterations to 6, 12, 18, 24, and 52 can achieve a BER of 10^{-1} , 10^{-2} , 10^{-3} , 10^{-4} , and 10^{-5} , respectively.

the last communication round, denoted as b_R , is set as a small value, i.e., 10^{-4} in our experiments. The concrete expression of b_r in our experiment is $b_r = \frac{0.0999R^2}{(R^2-1)r^2} + \frac{10^{-4}R^2-0.1}{R^2-1}$. For each communication round, the BER is scaled according to (7), and the corresponding maximum number of LDPC decoding iterations in that round is obtained from the lookup table.

Remark 2. Note that the number of entries in the lookup table depends on the possible discrete BER and SNR values. Since this number is not large, the memory overhead for storing the lookup table is expected to be small. Additionally, reading data from the lookup table takes constant time and does not introduce additional LDPC decoding latency.

IV. EXPERIMENTAL RESULTS

In this section, we validate the effectiveness of the proposed adaptive LDPC decoding algorithm via numerical experiments. First, we introduce the experimental settings. Then, the performance of the proposed algorithm, including test accuracy and energy consumption, is compared with a fixed-iteration LDPC decoding baseline.

A. Experimental Settings

System Setups: We consider an FL system with 10 clients. Clients are assumed active in every training round and they communicate with the server using rate 1/2 min-sum LDPC code with a code length of 1008 [47]. Besides, binary phase shift keying (BPSK) is adopted as the modulation scheme. In each training round, the number of local SGD steps is set as 5 with the learning rate and batch size as 0.01 and 64, respectively.

Datasets: We conduct experiments on three dataset, including MNIST [48], Fashion-MNIST [49], and CIFAR-10 [50]. The training datasets were distributed among mobile devices in an independent and identically distributed (IID) manner. We further consider one non-IID experiment on Fashion-MNIST

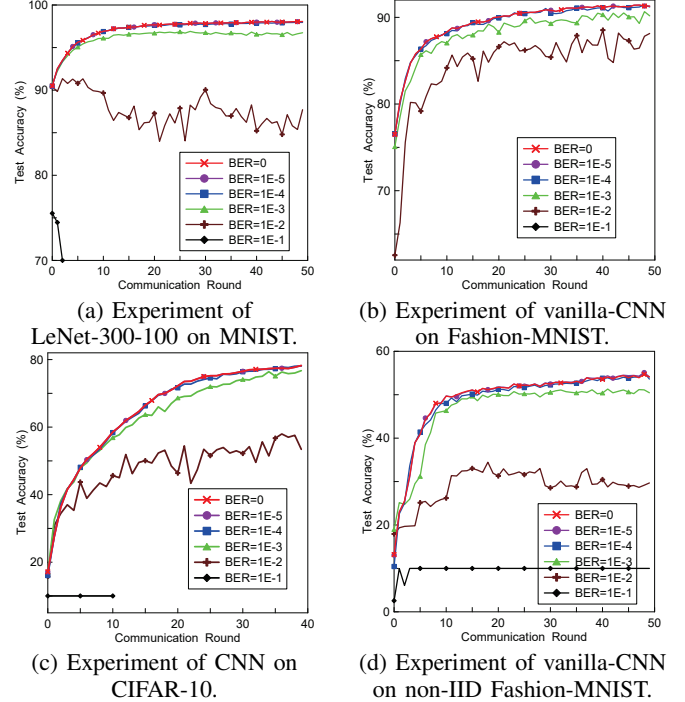


Fig. 5: Experiments on different datasets showing how fixed BER affects FL accuracy.

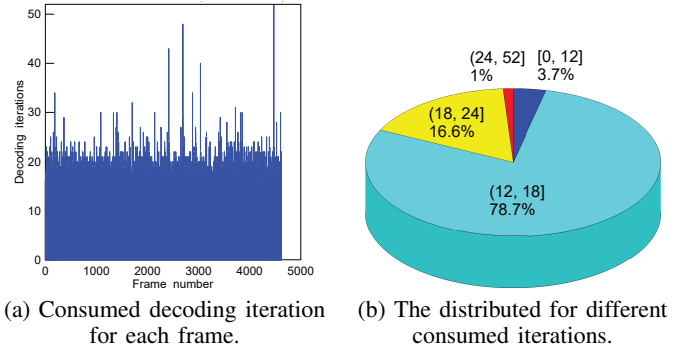


Fig. 6: Example of vanilla-CNN on Fashion-MNIST. The 8-bit quantized vanilla CNN model goes through AWGN channel with E_b/N_0 of 2.5dB, and is decoded by LDPC of block-length of 1008 bit.

where each client was assigned only two categories of training data, similar to the setup in [27]. The test datasets were utilized for validation on the server side.

DNN Models: For the MNIST dataset, the LeNet-300-100 model [51] is employed, which is a fully connected neural network consisting of two hidden layers and one softmax layer, with approximately 0.27 million parameters. For the Fashion-MNIST dataset, a vanilla CNN [3] with two 5×5 convolution layers, one fully connected layer, and one softmax layer is employed, comprising around 0.58 million parameters. For the CIFAR-10 dataset, a 7-layer CNN model with four 3×3 convolution layers, two fully connected layers, and one softmax layer is employed, which contains approximately 9.07 million parameters.

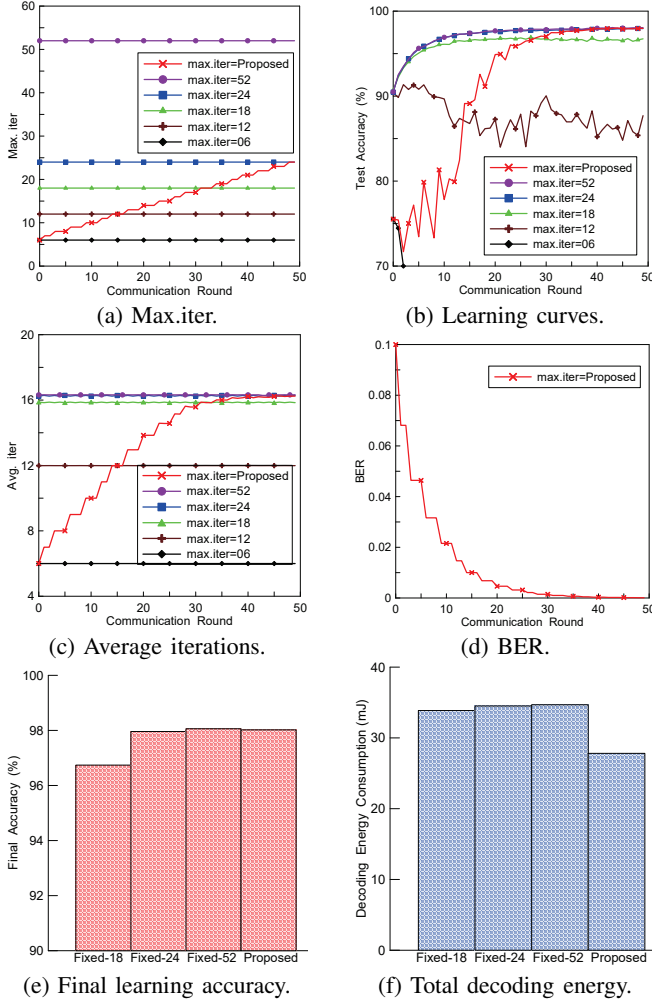


Fig. 7: Experiment for LeNet-300-100 on MNIST. Compared with the conventional fixed schemes, our method that adaptively increases the maximum decoding iteration to 24 can achieve the same final accuracy of 98%, and reduce the decoding energy by 6.7mJ.

B. Learning Performance of Conventional Schemes

In this subsection, the experimental results for conventional schemes that use fixed decoding iterations are presented. As shown in Fig. 4, the fixed decoding iterations lead to fixed BERs in the whole training process.

Next, the impact of fixed BER on FL performance was investigated. Fig. 5 summarizes the test accuracy with different fixed number of maximum decoding iterations. It can be observed that for all four FL tasks, when BER is higher than 10^{-3} , the learning performance was significantly impacted. Lowering the BER to 10^{-4} leads to improved accuracy and convergence towards perfect communication levels. However, further decreasing the BER to 10^{-5} will not yield any significant improvement in learning performance.

C. Learning Performance of the Proposed Approach

In this subsection, the proposed BER scaling algorithm is compared to the fixed BER scheme. The proposed approach

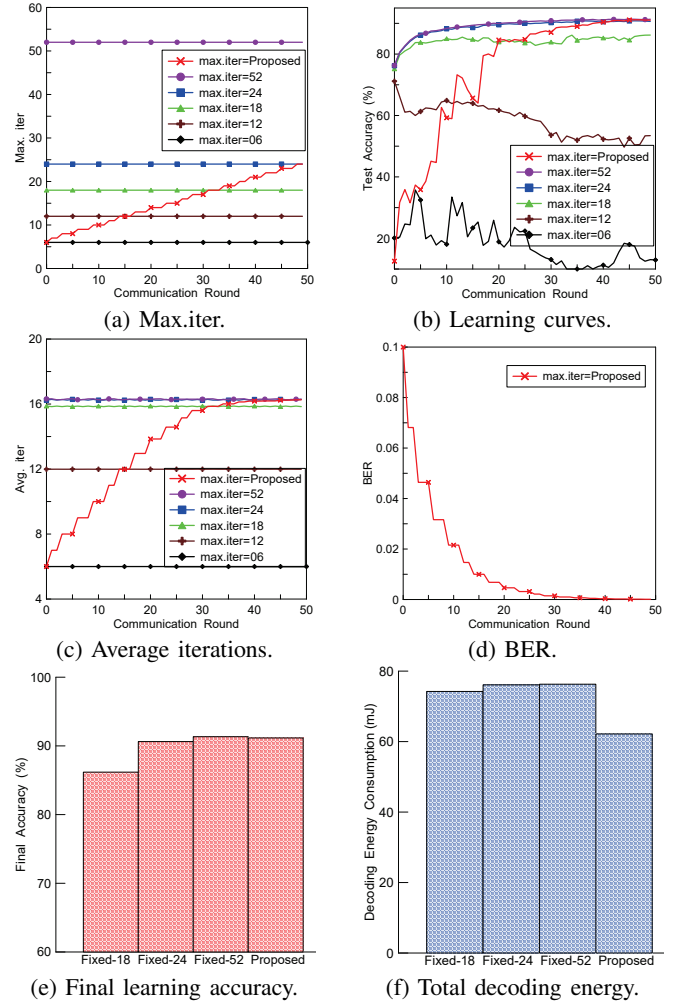


Fig. 8: Experiment for vanilla CNN on Fashion-MNIST. Compared with the conventional fixed schemes, our method that adaptively increases the maximum decoding iteration to 24 can achieve a similar final accuracy of 91%, and reduce the decoding energy by 14.1mJ.

uses a scaling BER of $\mathcal{O}(1/r^2)$ by controlling the maximum decoding iteration in each communication round based on a lookup table that summarizes the relationship between the BER and decoding iterations.

Specifically, the learning process is assigned with an initial BER value of 10^{-1} and a target BER value of 10^{-4} . Based on the BER scaling rule of $\mathcal{O}(1/r^2)$, the desired BER at every communication round can be calculated. Then based on the lookup table, we can control the LDPC maximum decoding iteration for every communication round. In the experiments, the initial and final maximum decoding iterations are set to 6 and 24, respectively. The learning performance and energy consumption of the proposed adaptive scheme are compared to those of fixed schemes with fixed BER of 10^{-4} . The corresponding fixed maximum decoding iterations is set to 24. To mitigate energy consumption, the LDPC decoder employs an early termination scheme, where the decoding process stops when the bitstream in a frame is deemed correct. Thus, only frames that cannot be correctly decoded require the maximum

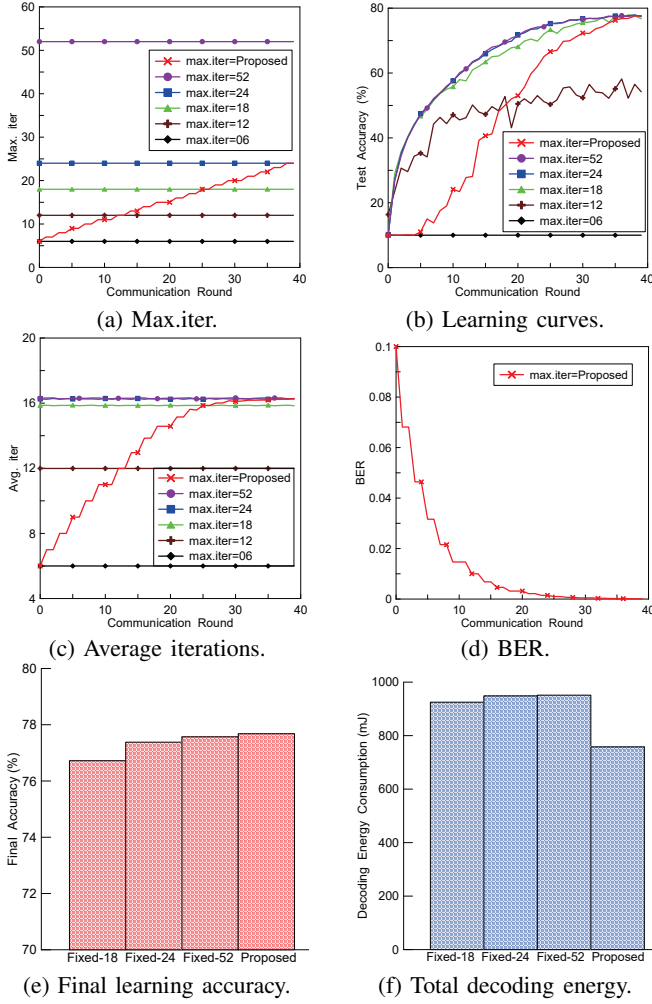


Fig. 9: Experiment for 7-layer CNN on CIFAR-10. Compared with the conventional fixed schemes, our method that adaptively increases the maximum decoding iteration to 24 can achieve a similar final accuracy of 77.6%, and reduce the decoding energy by 190mJ.

decoding iteration. Fig. 6 shows an example for the early termination scheme by using the experiment of vanilla-CNN on Fashion-MNIST, illustrating the actual decoding iterations for each bitstream. It can be observed that only a few bitstreams use up the maximum decoding iterations which is set to 52. The average decoding iterations is the average number of real consumed decoding iterations. Given the decoding energy is proportional to the decoding iterations, the decoding energy consumption can be reflected by the average number of decoding iterations used for the FL task.

Fig. 7 summarises the experimental results for LeNet-300-100 on MNIST. Fig. 7(a) shows how the maximum number of LDPC decoding iterations varies with the FL communication rounds for the proposed approach compared with other fixed schemes. The traditional schemes adopt a fixed number of maximum decoding iterations, resulting in a fixed BER, while the proposed scheme adopts a roughly linearly increasing number of maximum decoding iterations to achieve the designed BER. Fig. 7(b) shows the learning accuracy curves

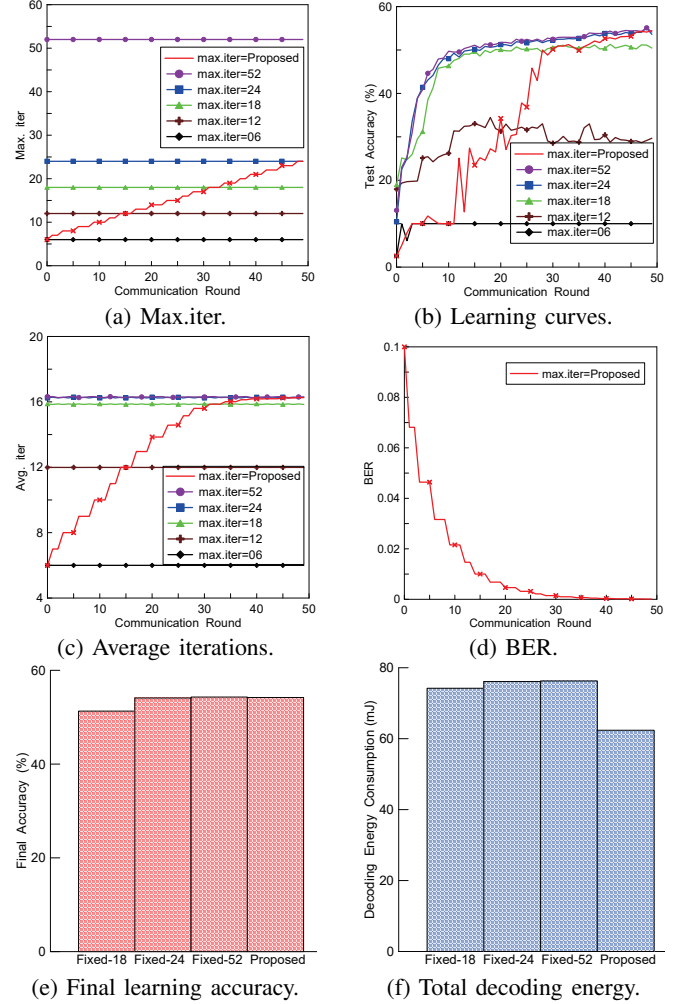


Fig. 10: Experiment for vanilla CNN on non-IID Fashion-MNIST. Compared with the conventional fixed schemes, our method that adaptively increases the maximum decoding iteration to 24 can achieve a similar final accuracy of 54.1%, and reduce the decoding energy by 13.9mJ.

for different schemes. Setting the fixed maximum decoding iteration to 6, which corresponds to a BER of 10^{-1} , severely affects the training accuracy. Similarly, when the maximum decoding iteration is set to 12, resulting in a BER of about 10^{-2} , the training still fails to converge. With a maximum decoding iteration of 18, corresponding to a BER of about 10^{-3} , the training can converge, but with a noticeable loss in accuracy. The training converges well to high learning accuracy when the maximum decoding iteration is increased to 24, resulting in a BER of 10^{-4} . Further increasing the maximum decoding iteration to 52 does not lead to further accuracy improvement.

The proposed scheme, which approximately increases the maximum decoding iteration from 6 to 24 in a linear manner, enables the training accuracy to improve rapidly and converge to the same level as the fixed scheme with 24/52 iterations. Fig. 7(c) illustrates how the average number of decoding iterations varies during training. The proposed scheme can reduce the average number of iterations and thus the overall

energy consumption. Fig. 7(d) depicts the BER of the proposed scheme, which scales as $\mathcal{O}(1/r^2)$ from 10^{-1} to 10^{-4} . Fig. 7(e) shows the final accuracy of different schemes. It can be observed that the proposed approach achieves the same accuracy as the fixed schemes that always maintain a very low BER of 10^{-4} and 10^{-5} throughout the training process. Fig. 7(f) illustrates the decoding energy consumption on the mobile side for the different schemes. It is obtained by multiplying the total number of LDPC decoding iterations with the LDPC decoding energy efficiency reported in [32]. Compared to the fixed schemes using a maximum decoding iteration of 24, the proposed scaling scheme can reduce the overall decoding energy by 19.4%.

Figs. 8, 9, and 10 present the experimental results for Fashion-MNIST, CIFAR-10, and non-IID Fashion-MNIST, respectively. The results are similar to those obtained by the MNIST experiment and show that the adaptive scheme can achieve similar or even slightly better accuracy compared to the fixed schemes. The observation of slightly better learning accuracy was also reported in [52]–[54], which suggests that adding noise to the model could enhance its generalization ability, and annealed noise could help achieve better learning accuracy. Overall, the proposed scheme reduces the LDPC decoding energy for Fashion-MNIST, CIFAR-10, and non-IID Fashion-MNIST by 18.3%, 20.1%, and 18.0%, respectively. Table III provides a summary of the experimental data.

V. CONCLUSION

In this paper, we considered the energy consumption issue in federated learning (FL) over digital communication networks. The study recognized that channel decoding contributes to a large portion of the energy consumption for mobile FL, which has not been previously highlighted. It was shown that, due to the robustness of FL to communication errors, properly control the BER over different communication rounds can achieve the same convergence rate as error-free FL. Based on this analysis, we proposed an energy-efficient LDPC decoding iteration control algorithm. Experimental results demonstrated that the proposed method can reduce approximately 20% the total energy consumed by LDPC decoding, while maintaining the same or even a slightly higher learning accuracy compared to the scheme without decoding iteration control.

APPENDIX

A. Proof of Theorem 1

Proof Outline: To prove Theorem 1, we first derive four lemmas, namely Lemmas 1–4, to establish the relationship between the convergence rate and model error. Then Lemma 5 builds the connection between model error and BER. By combining these relations, Theorem 1 is proved, which presents the relationship between convergence rate and BER.

TABLE III: Experimental Results of Different Schemes. Our scheme can achieve similar accuracy while saving around 20% of the decoding energy compared to the best-fixed scheme.

	Final learning accuracy			
	Fixed-18	Fixed-24	Fixed-52	Ours
MNIST	96.74%	97.96%	98.06%	98.02%
Fashion-MNIST	86.18%	90.63%	91.24%	91.16%
CIFAR-10	76.72%	77.38%	77.57%	77.68%
non-IID Fashion	51.3%	54.1%	54.3%	54.2%
Total consumed decoding energy (mJ)				
	Fixed-18	Fixed-24	Fixed-52	Ours
MNIST	33.87	34.51	34.68	27.81
Fashion-MNIST	74.23	76.10	76.29	62.17
CIFAR-10	925.10	948.44	951.36	757.80
non-IID Fashion	74.22	76.11	76.27	62.38

For each communication round $r = 1, \dots, R$ and local iteration $e = 1, \dots, E$, we have

$$\begin{aligned}
 \mathbf{w}_{r+1} &= \mathbf{w}_r + \frac{1}{s} \sum_{k \in S_r} (\mathbf{w}_{r,E}^k - (Q(\mathbf{w}_r))'), \\
 \hat{\mathbf{w}}_{r+1} &= \mathbf{w}_r + \frac{1}{n} \sum_{k \in [n]} (\mathbf{w}_{r,E}^k - (Q(\mathbf{w}_r))'), \\
 \bar{\mathbf{w}}_{r,e} &= \frac{1}{n} \sum_{k \in [n]} \mathbf{w}_{r,e}^k,
 \end{aligned} \tag{14}$$

where \mathbf{w}_{r+1} represents the updated global model based on s selected clients, $\hat{\mathbf{w}}_{r+1}$ denotes the updated global model based on all n clients, and $\bar{\mathbf{w}}_{r,e}$ denotes the average model of n local models. $(Q(\mathbf{w}_r))'$ represents that the downlink model \mathbf{w}_r will be impacted by the quantization operation $Q(\cdot)$ and channel noise $(\cdot)'$ before being received by the clients. To simplify the representation, we will use $Q'(\cdot)$ to replace $(Q(\cdot))'$ in subsequent derivations.

Lemma 1. Assuming that Assumptions 1 and 4 hold, for any communication round $r = 1, \dots, R$, we have

$$\begin{aligned}
 \mathbb{E}f(\mathbf{w}_{r+1}) &\leq \mathbb{E}f(\bar{\mathbf{w}}_{r,E}) + \frac{L}{2} \mathbb{E}\|\hat{\mathbf{w}}_{r+1} - \bar{\mathbf{w}}_{r,E}\|^2 \\
 &\quad + \frac{L}{2} \mathbb{E}\|\hat{\mathbf{w}}_{r+1} - \mathbf{w}_{r+1}\|^2.
 \end{aligned} \tag{15}$$

This lemma provides a bound on the training loss of the updated global model. This bound can be derived from the L -smooth property of the loss function on the server side. The proof is given in Appendix-B.

In the next three lemmas, we derive the upper bounds for the three terms on the RHS of (15).

Lemma 2. Assuming that Assumptions 1–3 hold and considering the sequence of updates with step size η , the following inequality holds for the case of noisy downlink transmission:

$$\begin{aligned}
 \mathbb{E}f(\bar{\mathbf{w}}_{r,E}) &\leq \frac{L}{2} \mathbb{E}\|Q'(\mathbf{w}_r) - \mathbf{w}_r\|^2 - \frac{\eta}{2} \sum_{e=1}^E \mathbb{E}\|\nabla f(\bar{\mathbf{w}}_{r,e})\|^2 \\
 &\quad + \mathbb{E}f(\mathbf{w}_r) - \frac{\eta}{2n} (1 - L\eta) \sum_{e=1}^E \sum_{k \in [n]} \mathbb{E}\|\nabla f(\mathbf{w}_{r,e}^k)\|^2 \\
 &\quad + \frac{LE\eta^2\sigma_L^2}{2n} + \frac{E\eta^2\sigma_G^2}{2}.
 \end{aligned} \tag{16}$$

The proof is given in Appendix-B. This lemma captures the process of noisy broadcasting and local updates. As shown in

the RHS of Eq.(16), the first two terms arise from the noisy broadcasting, while the subsequent terms come from the local training process.

Lemma 3. For $\hat{\mathbf{w}}_{r+1}$ and $\bar{\mathbf{w}}_{r,E}$ defined in (14), we have

$$\mathbb{E}\|\hat{\mathbf{w}}_{r+1} - \bar{\mathbf{w}}_{r,E}\|^2 = \mathbb{E}\|\mathbf{w}_r - Q'(\mathbf{w}_r)\|^2. \quad (17)$$

This lemma indicates that the expectation of the global model error on the server side is the same as the downlink model error on client side. The proof can be found in Appendix-B.

Lemma 4. For \mathbf{w}_{r+1} and $\hat{\mathbf{w}}_{r+1}$ defined in (14), we have

$$\mathbb{E}\|\mathbf{w}_{r+1} - \hat{\mathbf{w}}_{r+1}\|^2 \leq \frac{4}{s(n-1)}\left(1 - \frac{s}{n}\right) \cdot \left[\eta^2 \sigma_L^2 E n + \eta^2 E \sum_{e=1}^E \sum_{k \in [n]} \|\nabla f(\mathbf{w}_{r,e}^k)\|^2 \right]. \quad (18)$$

This lemma captures the effect of partial participation of clients. The proof is provided in Appendix-B.

By substituting Lemmas 2-4 into Lemma 1, we derive the following recursive inequality for the updated model at the server:

$$\begin{aligned} \mathbb{E}f(\mathbf{w}_{r+1}) &\leq L\mathbb{E}\|\mathbf{w}_r - Q'(\mathbf{w}_r)\|^2 - \frac{\eta}{2} \sum_{e=1}^E \mathbb{E}\|\nabla f(\bar{\mathbf{w}}_{r,e})\|^2 \\ &\quad - \frac{\eta}{2n} \left\{ 1 - L\eta - \frac{4LE(n-s)}{s(n-1)} \right\} \cdot \sum_{e=1}^E \sum_{k \in [n]} \mathbb{E}\|\nabla f(\mathbf{w}_{r,e}^k)\|^2 \\ &\quad + \mathbb{E}f(\mathbf{w}_r) + \frac{\eta E \sigma_G^2}{2} + L\eta^2 \sigma_L^2 E \left(\frac{1}{2n} + \frac{2(n-s)}{s(n-1)} \right). \end{aligned} \quad (19)$$

When η satisfies the condition

$$1 - L\eta - \frac{4LE(n-s)}{s(n-1)} \geq 0, \quad (20)$$

we have

$$\begin{aligned} \mathbb{E}f(\mathbf{w}_{r+1}) &\leq L\mathbb{E}\|\mathbf{w}_r - Q'(\mathbf{w}_r)\|^2 - \frac{\eta}{2} \sum_{e=1}^E \mathbb{E}\|\nabla f(\bar{\mathbf{w}}_{r,e})\|^2 \\ &\quad + \mathbb{E}f(\mathbf{w}_r) + \frac{E\eta^2 \sigma_G^2}{2} + L\eta^2 \sigma_L^2 E \left(\frac{1}{2n} + \frac{2(n-s)}{s(n-1)} \right). \end{aligned} \quad (21)$$

Summing (21) over $r = 1, \dots, R$ and rearranging the terms, we obtain the following expression:

$$\begin{aligned} \frac{\eta}{2} \sum_{r=1}^R \sum_{e=1}^E \mathbb{E}\|\nabla f(\bar{\mathbf{w}}_{r,e})\|^2 &\leq L \sum_{r=1}^R \mathbb{E}\|\mathbf{w}_r - Q'(\mathbf{w}_r)\|^2 \\ &\quad + f(\mathbf{w}_0) - f^* + \frac{RE\eta^2 \sigma_G^2}{2} + RL\eta^2 \sigma_L^2 E \left(\frac{1}{2n} + \frac{2(n-s)}{s(n-1)} \right). \end{aligned} \quad (22)$$

Multiplying $\frac{2}{RE\eta}$ on both sides of (22), we get

$$\begin{aligned} \frac{1}{RE} \sum_{r=1}^R \sum_{e=1}^E \mathbb{E}\|\nabla f(\bar{\mathbf{w}}_{r,e})\|^2 &\leq \frac{2L}{RE\eta} \sum_{r=1}^R \mathbb{E}\|\mathbf{w}_r - Q'(\mathbf{w}_r)\|^2 \\ &\quad + \frac{2(f(\mathbf{w}_0) - f^*)}{RE\eta} + \eta \sigma_G^2 + L\eta \sigma_L^2 \left(\frac{1}{n} + \frac{4(n-s)}{s(n-1)} \right). \end{aligned} \quad (23)$$

Since a high quantization bit-length is assumed to be used in this work with negligible quantization error, we have

$$\begin{aligned} \mathbb{E}\|\mathbf{w}_r - Q'(\mathbf{w}_r)\|^2 &= \mathbb{E}\|Q'(\mathbf{w}_r) - Q(\mathbf{w}_r) + Q(\mathbf{w}_r) - \mathbf{w}_r\|^2 \\ &= \mathbb{E}\|(\mathbf{w}_r)' - \mathbf{w}_r\|^2. \end{aligned} \quad (24)$$

Combining (23) and (24), we obtain

$$\begin{aligned} \frac{1}{RE} \sum_{r=1}^R \sum_{e=1}^E \mathbb{E}\|\nabla f(\bar{\mathbf{w}}_{r,e})\|^2 &\leq \frac{2L}{RE\eta} \sum_{r=1}^R \mathbb{E}\|(\mathbf{w}_r)' - \mathbf{w}_r\|^2 \\ &\quad + \frac{2(f(\mathbf{w}_0) - f^*)}{RE\eta} + \eta \sigma_G^2 + L\eta \sigma_L^2 \left(\frac{1}{n} + \frac{4(n-s)}{s(n-1)} \right). \end{aligned} \quad (25)$$

Lemma 5. For the perfect global model \mathbf{w} and the received noisy model $(\mathbf{w})'$, the model error can be bounded by

$$\mathbb{E}\|(\mathbf{w})' - \mathbf{w}\|^2 \leq \frac{4d(4^N - 1)}{3(2^N - 1)^2} \cdot b \cdot M^2, \quad (26)$$

where M denotes the maximum absolute value among all weight elements, i.e. $M = \max(|w_1|, |w_2|, \dots, |w_d|)$. Lemma 5 gives the relationship between model variance and BER. The proof can be found in Appendix-B.

By substituting Eq.(26) into Eq.(25), we establish the relationship between the FL convergence rate and BER:

$$\begin{aligned} \frac{1}{RE} \sum_{r=1}^R \sum_{e=1}^E \mathbb{E}\|\nabla f(\bar{\mathbf{w}}_{r,e})\|^2 &\leq \frac{8LdM^2}{3RE\eta} \sum_{r=1}^R \frac{b_r(4^N - 1)}{(2^N - 1)^2} \\ &\quad + \frac{2(f(\mathbf{w}_0) - f^*)}{RE\eta} + \eta \sigma_G^2 + L\eta \sigma_L^2 \left(\frac{1}{n} + \frac{4(n-s)}{s(n-1)} \right). \end{aligned} \quad (27)$$

When the quantization bit-length is high, we have $\frac{4^N - 1}{(2^N - 1)^2} \approx 1$, and Eq.(27) can be simplified as follows:

$$\begin{aligned} \frac{1}{RE} \sum_{r=1}^R \sum_{e=1}^E \mathbb{E}\|\nabla f(\bar{\mathbf{w}}_{r,e})\|^2 &\leq \frac{2(f(\mathbf{w}_0) - f^*)}{RE\eta} \\ &\quad + \frac{8LdM^2}{3RE\eta} \sum_{r=1}^R b_r + L\eta \sigma_L^2 \left(\frac{1}{n} + \frac{4(n-s)}{s(n-1)} \right) + \eta \sigma_G^2, \end{aligned} \quad (28)$$

which completes the proof of Theorem 1.

B. Proof of Lemmas

1) Proof of Lemma 1

Quantization is unbiased according to Assumption 3, i.e., $\mathbb{E}_Q(\mathbf{w}) = \mathbf{w}$. It is proved in Eq.(44) that the impact of the BER is also unbiased. So we have $\mathbb{E}_{Q'}Q'(\mathbf{w}) = \mathbf{w}$. Based on the above unbiased properties and the notations defined in Eq.(14), we have

$$\begin{aligned} \mathbb{E}_{Q'}\hat{\mathbf{w}}_{r+1} &= \mathbf{w}_r + \frac{1}{n} \sum_{k \in [n]} (\mathbf{w}_{r,E}^k - \mathbb{E}_{Q'}Q'(\mathbf{w}_r)) \\ &= \mathbf{w}_r + \frac{1}{n} \sum_{k \in [n]} (\mathbf{w}_{r,E}^k - \mathbf{w}_r) \\ &= \frac{1}{n} \sum_{k \in [n]} \mathbf{w}_{r,E}^k \\ &= \bar{\mathbf{w}}_{r,E}. \end{aligned} \quad (29)$$

We can also get

$$\mathbb{E}_{S_r}\mathbf{w}_{r+1} = \mathbf{w}_r + \frac{1}{n} \sum_{k \in [n]} (\mathbf{w}_{r,E}^k - Q'(\mathbf{w}_r)) = \hat{\mathbf{w}}_{r+1}, \quad (30)$$

whose proof is similar to Section 7.1 in [35].

Since the loss function f is L -smooth, for any variables \mathbf{x}, \mathbf{y} , we have

$$f(\mathbf{x}) \leq f(\mathbf{y}) + \langle \nabla f(\mathbf{y}), \mathbf{x} - \mathbf{y} \rangle + \frac{L}{2} \|\mathbf{x} - \mathbf{y}\|^2. \quad (31)$$

Taking $\mathbf{x} = \hat{\mathbf{w}}_{r+1}$ and $\mathbf{y} = \bar{\mathbf{w}}_{r,E}$ in (31), we can get

$$f(\hat{\mathbf{w}}_{r+1}) \leq f(\bar{\mathbf{w}}_{r,E}) + \langle \nabla f(\bar{\mathbf{w}}_{r,E}), \hat{\mathbf{w}}_{r+1} - \bar{\mathbf{w}}_{r,E} \rangle + \frac{L}{2} \|\hat{\mathbf{w}}_{r+1} - \bar{\mathbf{w}}_{r,E}\|^2. \quad (32)$$

We take the expectation on both sides of (32) and, since $\mathbb{E}_{Q'} \hat{\mathbf{w}}_{r+1} = \bar{\mathbf{w}}_{r,E}$ (see (29)), we have

$$\mathbb{E}f(\hat{\mathbf{w}}_{r+1}) \leq \mathbb{E}f(\bar{\mathbf{w}}_{r,E}) + \frac{L}{2} \mathbb{E}\|\hat{\mathbf{w}}_{r+1} - \bar{\mathbf{w}}_{r,E}\|^2. \quad (33)$$

Taking $\mathbf{x} = \mathbf{w}_{r+1}$ and $\mathbf{y} = \hat{\mathbf{w}}_{r+1}$ in (31), and following the same steps as in (32) and (33), we have

$$\mathbb{E}f(\mathbf{w}_{r+1}) \leq \mathbb{E}f(\hat{\mathbf{w}}_{r+1}) + \frac{L}{2} \mathbb{E}\|\hat{\mathbf{w}}_{r+1} - \mathbf{w}_{r+1}\|^2. \quad (34)$$

By combining (33) and (34), we can get Lemma 1.

2) Proof of Lemma 2

Based on the proof in Section 8.3 of [35], and considering the non-iid case as in Assumption 3, if the downlink communication is perfect, we can obtain the upper bound of FL convergence as

$$\begin{aligned} \mathbb{E}f(\bar{\mathbf{w}}_{r,E}) &\leq \mathbb{E}f(\mathbf{w}_r) - \frac{\eta}{2} \sum_{e=1}^E \mathbb{E}\|\nabla f(\bar{\mathbf{w}}_{r,e})\|^2 \\ &\quad - \eta \left(\frac{1}{2n} - \frac{L\eta}{2n} - \frac{L^2\eta^2 E(E-1)}{n} \right) \sum_{e=1}^E \sum_{k \in [n]} \mathbb{E}\|\nabla f(\mathbf{w}_{r,e}^k)\|^2 \\ &\quad + \frac{LE\eta^2\sigma_L^2}{2n} + \frac{L^2\eta^3\sigma_L^2(n+1)E(E-1)}{2n}. \end{aligned} \quad (35)$$

For noisy downlink communication, the received model will have quantization and BER noise. As a result, (35) can be rewritten as

$$\begin{aligned} \mathbb{E}f(\bar{\mathbf{w}}_{r,E}) &\leq \mathbb{E}f(Q'(\mathbf{w}_r)) - \frac{\eta}{2} \sum_{e=1}^E \mathbb{E}\|\nabla f(\bar{\mathbf{w}}_{r,e})\|^2 \\ &\quad - \eta \left(\frac{1}{2n} - \frac{L\eta}{2n} - \frac{L^2\eta^2 E(E-1)}{n} \right) \sum_{e=1}^E \sum_{k \in [n]} \mathbb{E}\|\nabla f(\mathbf{w}_{r,e}^k)\|^2 \\ &\quad + \frac{LE\eta^2\sigma_L^2}{2n} + \frac{E\eta^2\sigma_G^2}{2}. \end{aligned} \quad (36)$$

Since f is L -smooth, according to (31), we have

$$f(Q'(\mathbf{w}_r)) \leq f(\mathbf{w}_r) + \langle \nabla f(\mathbf{w}_r), Q'(\mathbf{w}_r) - \mathbf{w}_r \rangle + \frac{L}{2} \|Q'(\mathbf{w}_r) - \mathbf{w}_r\|^2. \quad (37)$$

Since the quantization and BER are both unbiased, i.e., $\mathbb{E}_{Q'} Q'(\mathbf{w}) = \mathbb{E}_Q Q(\mathbf{w}) = \mathbf{w}$, we take the expectation on both sides of (37) to obtain

$$\mathbb{E}f(Q'(\mathbf{w}_r)) \leq \mathbb{E}f(\mathbf{w}_r) + \frac{L}{2} \mathbb{E}\|Q'(\mathbf{w}_r) - \mathbf{w}_r\|^2. \quad (38)$$

Combining (36) and (38), we prove Lemma 2.

3) Proof of Lemma 3

According to the notations defined in Eq.(14), we can get the

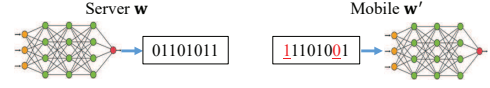


Fig. 11: The difference between received noisy model and broadcasted perfect global model.

expanded representation of $\hat{\mathbf{w}}_{r+1}$ and $\bar{\mathbf{w}}_{r,E}$ and derive

$$\begin{aligned} &\mathbb{E}\|\hat{\mathbf{w}}_{r+1} - \bar{\mathbf{w}}_{r,E}\|^2 \\ &= \mathbb{E}\|\mathbf{w}_r + \frac{1}{n} \sum_{k \in [n]} (\mathbf{w}_{r,E}^k - Q'(\mathbf{w}_r)) - \frac{1}{n} \sum_{k \in [n]} \mathbf{w}_{r,E}^k\|^2 \\ &= \mathbb{E}\|\mathbf{w}_r + \frac{1}{n} \sum_{k \in [n]} \mathbf{w}_{r,E}^k - \frac{1}{n} \sum_{k \in [n]} Q'(\mathbf{w}_r) - \frac{1}{n} \sum_{k \in [n]} \mathbf{w}_{r,E}^k\|^2 \\ &= \mathbb{E}\|\mathbf{w}_r - Q'(\mathbf{w}_r)\|^2, \end{aligned} \quad (39)$$

which concludes the proof of Lemma 3.

4) Proof of Lemma 4

Similar to Section 8.5 in [35] and considering the noise in the downlink global model, we have

$$\begin{aligned} \mathbb{E}\|\mathbf{w}_{r+1} - \hat{\mathbf{w}}_{r+1}\|^2 &\leq \frac{4}{s(n-1)} \left(1 - \frac{s}{n}\right) \\ &\quad \sum_{k \in [n]} \mathbb{E}\|\mathbf{w}_{r,E}^k - Q'(\mathbf{w}_r)\|^2. \end{aligned} \quad (40)$$

Based on E steps of local training with learning rate η , we have

$$\mathbb{E}\|\mathbf{w}_{r,E}^k - Q'(\mathbf{w}_r)\|^2 \leq \eta^2 E (\sigma_L^2 + \sum_{e=1}^E \|\nabla f(\mathbf{w}_{r,e}^k)\|^2). \quad (41)$$

Combining (40) and (41), we can conclude Lemma 4.

5) Proof of Lemma 5

Due to communication errors, the received DNN model for local training will contain random errors and differ from the global model, as shown in Fig. 11. In the following, we analyze the effect of the BER on the model error.

For a quantization scheme using N bits to represent the weight w , the probability of having x bit errors is given by

$$P(X = x) = C_N^x b^x (1-b)^{N-x}. \quad (42)$$

Since b is much smaller than 1, the following relations can be established:

$$P(X = 0) \gg P(X = 1) \gg P(X = 2) \gg \dots \gg P(X = 8). \quad (43)$$

Therefore, the focus is on the case with at most one error bit.

The bit error can occur at various positions, ranging from the Least Significant Bit (LSB) to the Most Significant Bit (MSB), leading to different levels of error. For instance, for unsigned quantization, if the erroneous bit appears in the MSB and flips from 0 to 1, the error would be $+2^{N-1}\Delta$, where $\Delta = \frac{\max(\mathbf{w}) - \min(\mathbf{w})}{2^N - 1} = \frac{\text{range}(\mathbf{w})}{2^N - 1}$, denoting the bin value for a given quantization. Alternatively, if the MSB flips from 1 to 0, the quantified error will be $-2^{N-1}\Delta$. The results for the case that the error occurs at the LSB will be $+2^0\Delta$ and $-2^0\Delta$. Additionally, it is assumed that the numbers of 0 and 1 in the bitstreams are similar. Based on this analysis, we

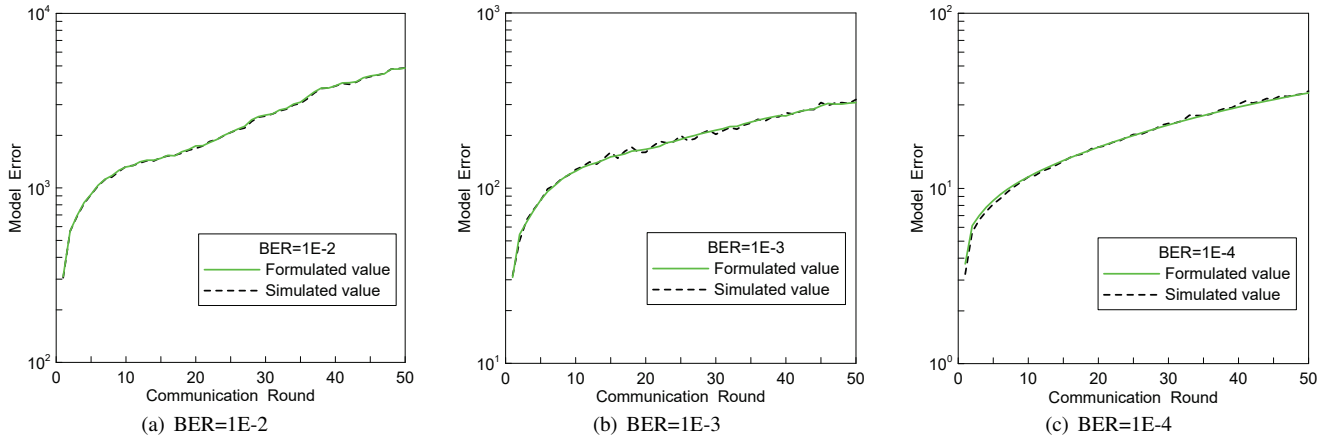


Fig. 12: Validation of the model error formula.

can determine all the cases of bit flipping, and calculate the resulting values of the noisy weight with the corresponding probabilities, as shown in Table IV.

TABLE IV: Probability mass function of $(w)'$.

$(w)'_i$	$w + 2^0\Delta$	$w - 2^0\Delta$	$w + 2^1\Delta$	$w - 2^1\Delta$
P_i	b/2	b/2	b/2	b/2
$(w)'_i$...	$w + 2^{N-1}\Delta$	$w - 2^{N-1}\Delta$	w
P_i	...	b/2	b/2	1-N·b

Based on Table IV, the mean and variance of the received noisy weight $(w)'$ can be calculated as follows:

$$\mathbb{E}((w)') = \sum_i ((w)'_i \cdot P_i) = w, \quad (44)$$

$$\begin{aligned} \mathbb{E}|| (w)' - w ||^2 &= \sum_i [((w)'_i - w)^2 \cdot P_i] \\ &= \frac{4^N - 1}{3(2^N - 1)^2} \cdot b \cdot \text{range}(\mathbf{w})^2. \end{aligned} \quad (45)$$

The above equations indicate that, for a weight parameter in the DNN model, the mean value of the noisy parameter is equal to the broadcasted perfect parameter. Furthermore, the variance between the two parameters is a function of the number of quantization bits, the BER level, and the range of the model parameters. For a d -dimensional model \mathbf{w} , i.e., $\mathbf{w} = [w_1, w_2, \dots, w_d]$, the following equations can be derived:

$$\begin{aligned} \mathbb{E}|| (\mathbf{w})' - \mathbf{w} ||^2 &= \sum_{j=1}^d \mathbb{E}|| (w_j)' - w_j ||^2 \\ &= \frac{(4^N - 1)d}{3(2^N - 1)^2} \cdot b \cdot \text{range}(\mathbf{w})^2. \end{aligned} \quad (46)$$

To verify the theoretical results of Eq.(46), simulations were conducted using an 8-bit vanilla-CNN on the Fashion-MNIST dataset. The experimental settings are described in Section IV-A. Three different BER conditions were simulated, and the model errors obtained from the simulation are plotted in Fig. 12. The expectation on the left-hand side (LHS) of Eq.(46) corresponds to different cases of errors. The model errors predicted using the proposed formula on the RHS of Eq.(46) are also plotted in the same figure. It can be seen

that, for different BER conditions and different communication rounds, the results obtained from the theoretical formula closely match those obtained from simulation, confirming the accuracy of the derived Eq.(46).

If we denote M as the maximum absolute value of all weight elements, i.e. $M = \max(|w_1|, |w_2|, \dots, |w_d|)$, we have $\text{range}(\mathbf{w}) \leq 2M$. The upper bound of Eq.(46) can be obtained as follows:

$$\mathbb{E}|| (\mathbf{w})' - \mathbf{w} ||^2 \leq \frac{4d(4^N - 1)}{3(2^N - 1)^2} \cdot b \cdot M^2, \quad (47)$$

which concludes the proof of Lemma 5.

REFERENCES

- [1] Y. LeCun, Y. Bengio, and G. Hinton, "Deep learning," *Nature*, vol. 521, no. 7553, pp. 436–444, 2015.
- [2] Q. Yang, Y. Liu, Y. Cheng, Y. Kang, T. Chen, and H. Yu, "Federated learning," *Synthesis Lectures on Artificial Intelligence and Machine Learning*, vol. 13, no. 3, pp. 1–207, 2019.
- [3] B. McMahan, E. Moore, D. Ramage, S. Hampson, and B. A. y Arcas, "Communication-efficient learning of deep networks from decentralized data," in *Artificial Intelligence and Statistics*. PMLR, 2017, pp. 1273–1282.
- [4] Z. Chai, H. Fayyaz, Z. Fayyaz, A. Anwar, Y. Zhou, N. Baracaldo, H. Ludwig, and Y. Cheng, "Towards taming the resource and data heterogeneity in federated learning.," in *OpML*, 2019, pp. 19–21.
- [5] Y. Laguel, K. Pillutla, J. Malick, and Z. Harchaoui, "Device heterogeneity in federated learning: A superquantile approach," *arXiv preprint arXiv:2002.11223*, 2020.
- [6] Z. Xie and S. Song, "Fedkl: Tackling data heterogeneity in federated reinforcement learning by penalizing kl divergence," *IEEE Journal on Selected Areas in Communications*, vol. 41, no. 4, pp. 1227–1242, 2023.
- [7] M. Chen, N. Shlezinger, H. V. Poor, Y. C. Eldar, and S. Cui, "Communication-efficient federated learning," *Proceedings of the National Academy of Sciences*, vol. 118, no. 17, pp. e2024789118, 2021.
- [8] M. Kim, W. Saad, M. Mozaffari, and M. Debbah, "Green, quantized federated learning over wireless networks: An energy-efficient design," *IEEE Transactions on Wireless Communications*, 2023.
- [9] Y. G. Kim and C.-J. Wu, "AutoFL: Enabling heterogeneity-aware energy efficient federated learning," in *MICRO-54: 54th Annual IEEE/ACM International Symposium on Microarchitecture*, 2021, pp. 183–198.
- [10] N. H. Tran, W. Bao, A. Zomaya, M. N. Nguyen, and C. S. Hong, "Federated learning over wireless networks: Optimization model design and analysis," in *IEEE INFOCOM 2019-IEEE Conference on Computer Communications*. IEEE, 2019, pp. 1387–1395.
- [11] P. Han, S. Wang, and K. K. Leung, "Adaptive gradient sparsification for efficient federated learning: An online learning approach," in *2020 IEEE 40th International Conference on Distributed Computing Systems (ICDCS)*. IEEE, 2020, pp. 300–310.

- [12] S. Zheng, C. Shen, and X. Chen, "Design and analysis of uplink and downlink communications for federated learning," *IEEE Journal on Selected Areas in Communications*, vol. 39, no. 7, pp. 2150–2167, 2020.
- [13] S. Chen, C. Shen, L. Zhang, and Y. Tang, "Dynamic aggregation for heterogeneous quantization in federated learning," *IEEE Transactions on Wireless Communications*, vol. 20, no. 10, pp. 6804–6819, 2021.
- [14] Y. Wang, Y. Xu, Q. Shi, and T.-H. Chang, "Quantized federated learning under transmission delay and outage constraints," *IEEE Journal on Selected Areas in Communications*, vol. 40, no. 1, pp. 323–341, 2021.
- [15] C. Shen and S. Chen, "Federated learning with heterogeneous quantization," in *2020 IEEE/ACM Symposium on Edge Computing (SEC)*. IEEE, 2020, pp. 405–409.
- [16] S. Chen, L. Li, G. Wang, M. Pang, and C. Shen, "Federated learning with heterogeneous quantization bit allocation and aggregation for internet of things," *IEEE Internet of Things Journal*, 2023.
- [17] L. Qu, S. Song, and C.-Y. Tsui, "FedDQ: Communication-efficient federated learning with descending quantization," in *GLOBECOM 2022-2022 IEEE Global Communications Conference*. IEEE, 2022, pp. 281–286.
- [18] M. Chen, Z. Yang, W. Saad, C. Yin, H. V. Poor, and S. Cui, "A joint learning and communications framework for federated learning over wireless networks," *IEEE Transactions on Wireless Communications*, vol. 20, no. 1, pp. 269–283, 2020.
- [19] S. Wang, M. Chen, W. Saad, and C. Yin, "Federated learning for energy-efficient task computing in wireless networks," in *ICC 2020-2020 IEEE International Conference on Communications (ICC)*. IEEE, 2020, pp. 1–6.
- [20] X. Qiu, J. Fernandez-Marques, P. P. Gusmao, Y. Gao, T. Parcollet, and N. D. Lane, "ZeroFl: Efficient on-device training for federated learning with local sparsity," *arXiv preprint arXiv:2208.02507*, 2022.
- [21] M. A. Raihan and T. Aamodt, "Sparse weight activation training," *Advances in Neural Information Processing Systems*, vol. 33, pp. 15625–15638, 2020.
- [22] I. Hubara, M. Courbariaux, D. Soudry, R. El-Yaniv, and Y. Bengio, "Quantized neural networks: Training neural networks with low precision weights and activations," *The Journal of Machine Learning Research*, vol. 18, no. 1, pp. 6869–6898, 2017.
- [23] Z. Yang, M. Chen, W. Saad, C. S. Hong, and M. Shikh-Bahaei, "Energy efficient federated learning over wireless communication networks," *IEEE Transactions on Wireless Communications*, vol. 20, no. 3, pp. 1935–1949, 2020.
- [24] M. Kim, W. Saad, M. Mozaffari, and M. Debbah, "On the tradeoff between energy, precision, and accuracy in federated quantized neural networks," in *ICC 2022-IEEE International Conference on Communications*. IEEE, 2022, pp. 2194–2199.
- [25] W. Tong and G. Y. Li, "Nine challenges in artificial intelligence and wireless communications for 6G," *IEEE Wireless Communications*, 2022.
- [26] X. Li, K. Huang, W. Yang, S. Wang, and Z. Zhang, "On the convergence of FedAvg on non-IID data," *arXiv preprint arXiv:1907.02189*, 2019.
- [27] T. Li, A. K. Sahu, M. Zaheer, M. Sanjabi, A. Talwalkar, and V. Smith, "Federated optimization in heterogeneous networks," *Proceedings of Machine Learning and Systems*, vol. 2, pp. 429–450, 2020.
- [28] D. Jhunjunwala, A. Gadhikar, G. Joshi, and Y. C. Eldar, "Adaptive quantization of model updates for communication-efficient federated learning," in *ICASSP 2021-2021 IEEE International Conference on Acoustics, Speech and Signal Processing (ICASSP)*. IEEE, 2021, pp. 3110–3114.
- [29] A. Krizhevsky, I. Sutskever, and G. E. Hinton, "Imagenet classification with deep convolutional neural networks," *Advances in Neural Information Processing Systems*, vol. 25, 2012.
- [30] S. Choi, J. Sim, M. Kang, Y. Choi, H. Kim, and L.-S. Kim, "An energy-efficient deep convolutional neural network training accelerator for in situ personalization on smart devices," *IEEE Journal of Solid-State Circuits*, vol. 55, no. 10, pp. 2691–2702, 2020.
- [31] X. Huang, H. Jia, S. Dong, W. Deng, Z. Wang, and B. Chi, "A 24-30GHz 4-element phased array transceiver with low insertion loss compact T/R switch and bidirectional phase shifter in 65 nm CMOS technology," in *2021 IEEE Asian Solid-State Circuits Conference (A-SSCC)*. IEEE, 2021, pp. 1–3.
- [32] W. Tang, C.-H. Chen, and Z. Zhang, "A 2.4-mm² 130-mW MMSE-nonbinary LDPC iterative detector decoder for 4×4 256-QAM MIMO in 65-nm CMOS," *IEEE Journal of Solid-State Circuits*, vol. 54, no. 7, pp. 2070–2080, 2019.
- [33] W. E. Ryan et al., "An introduction to LDPC codes," *CRC Handbook for Coding and Signal Processing for Recording Systems*, vol. 5, no. 2, pp. 1–23, 2004.
- [34] K. Nam-Il and K. Jin-Up, "Early termination scheme for 5g nr ldpc code," in *2021 International Conference on Information and Communication Technology Convergence (ICTC)*. IEEE, 2021, pp. 933–935.
- [35] A. Reiszadeh, A. Mokhtari, H. Hassani, A. Jadbabaie, and R. Pedarsani, "FedPAQ: A communication-efficient federated learning method with periodic averaging and quantization," in *International Conference on Artificial Intelligence and Statistics*. PMLR, 2020, pp. 2021–2031.
- [36] F. Ang, L. Chen, N. Zhao, Y. Chen, W. Wang, and F. R. Yu, "Robust federated learning with noisy communication," *IEEE Transactions on Communications*, vol. 68, no. 6, pp. 3452–3464, 2020.
- [37] M. M. Amiri, D. Gündüz, S. R. Kulkarni, and H. V. Poor, "Convergence of federated learning over a noisy downlink," *IEEE Transactions on Wireless Communications*, vol. 21, no. 3, pp. 1422–1437, 2021.
- [38] M. M. Amiri and D. Gündüz, "Federated learning over wireless fading channels," *IEEE Transactions on Wireless Communications*, vol. 19, no. 5, pp. 3546–3557, 2020.
- [39] X. Wei and C. Shen, "Federated learning over noisy channels," in *ICC 2021-IEEE International Conference on Communications*. IEEE, 2021, pp. 1–6.
- [40] X. Wei and C. Shen, "Federated learning over noisy channels: Convergence analysis and design examples," *IEEE Transactions on Cognitive Communications and Networking*, 2022.
- [41] T. Sery, N. Shlezinger, K. Cohen, and Y. C. Eldar, "Over-the-air federated learning from heterogeneous data," *IEEE Transactions on Signal Processing*, vol. 69, pp. 3796–3811, 2021.
- [42] Y. Sun, Z. Lin, Y. Mao, S. Jin, and J. Zhang, "Channel and gradient-importance aware device scheduling for over-the-air federated learning," *IEEE Transactions on Wireless Communications*, 2023.
- [43] H. Yang, M. Fang, and J. Liu, "Achieving linear speedup with partial worker participation in non-iid federated learning," *Proceedings of ICLR*, 2021.
- [44] A. Khandekar and R. McEliece, "On the complexity of reliable communication on the erasure channel," in *IEEE International Symposium on Information Theory*, 2001, pp. 1–1.
- [45] D. J. MacKay, "Good error-correcting codes based on very sparse matrices," *IEEE Transactions on Information Theory*, vol. 45, no. 2, pp. 399–431, 1999.
- [46] B. Lu, G. Yue, and X. Wang, "Performance analysis and design optimization of LDPC-coded MIMO OFDM systems," *IEEE Transactions on Signal Processing*, vol. 52, no. 2, pp. 348–361, 2004.
- [47] J. Sha, Z. Wang, M. Gao, and L. Li, "Multi-Gb/s LDPC code design and implementation," *IEEE Transactions on Very Large Scale Integration (VLSI) Systems*, vol. 17, no. 2, pp. 262–268, 2008.
- [48] Y. LeCun, "The MNIST database of handwritten digits," [Online]. Available: <http://yann.lecun.com/exdb/mnist/>, 1998.
- [49] H. Xiao, K. Rasul, and R. Vollgraf, "Fashion-MNIST: A novel image dataset for benchmarking machine learning algorithms," *arXiv preprint arXiv:1708.07747*, 2017.
- [50] A. Krizhevsky, V. Nair, and G. Hinton, "Cifar-10 (Canadian institute for advanced research)," URL <http://www.cs.toronto.edu/kriz/cifar.html>, vol. 5, no. 4, pp. 1, 2010.
- [51] S. Han, H. Mao, and W. J. Dally, "Deep compression: Compressing deep neural networks with pruning, trained quantization and Huffman coding," *arXiv preprint arXiv:1510.00149*, 2015.
- [52] A. Graves, "Practical variational inference for neural networks," *Advances in Neural Information Processing Systems*, vol. 24, 2011.
- [53] S. Hochreiter and J. Schmidhuber, "Simplifying neural nets by discovering flat minima," *Advances in Neural Information Processing Systems*, vol. 7, 1994.
- [54] A. Neelakantan, L. Vilnis, Q. V. Le, I. Sutskever, L. Kaiser, K. Kurach, and J. Martens, "Adding gradient noise improves learning for very deep networks," *arXiv preprint arXiv:1511.06807*, 2015.